UDK 539.3

V. D. Kubenko[1], M. V. Ayzenberg-Stepanenko[2]

IMPACT INDENTATION OF A RIGID BODY INTO AN ELASTIC LAYER. ANALYTICAL AND NUMERICAL APPROACHES*

A plane contact-impact problem is considered for an elastic layer subjected to indentation of a rigid body moving with a given velocity. An exact analytical solution is obtained in the case of a blunt contour of the indenter shape. Results of the solution are presented for stresses developed with time in a layer of a finite thickness. Stress pattern under multiple reflections is analyzed. A numerical solution of the problem is obtained on the basis of the simplified model of the elasticity theory having a single displacement. The explicit finite difference algorithm is developed on the basis of the mesh dispersion minimization technique resulting in precise calculations of discontinuities. Calculated stresses and force of resistance to pressing are presented in the cases of irregular shapes of the indenter contour (rectangle, wedge and their combination).

1. Introduction. Impact interaction of a rigid body with deformable media and structures is a topical subject of contemporary solid mechanics. Of the large number of publications devoted to this problem, only the generalizing works are cited herein. Review [24] presents the state of investigations using numerical approaches (primarily the method of finite elements). Monograph [1] is devoted to the development of analytical approaches to the solution of problems about the action of impact on an elastic medium. A generalizing monograph in the field of contact interaction [4] and a review [2] reflect the multitude of approaches to the study of a body's impact interaction with elastic and liquid media. In the general case the indentation problem is formulated as a non-stationary mixed initially-boundary problem of theory of elasticity with an *a priori* unknown (temporally varying) boundary, which must be determined in the course of the solution. The problem statement includes:

- equations of dynamic deformation of the impacted solid;
- the motion equation of the indenter;
- the ratio presenting the resistive force (drag) as a function of *a priori* unknown dimensions of the contact zone and surface stresses;
- the equation connecting the contact zone size with the indenter displacement;
- the corresponding boundary and initial conditions.

* This research was supported by the Center of Advanced Studies of Mathematics at Ben-Gurion University of the Negev.

The overwhelming majority of publications (at least of those in which analytical methods are used) are devoted to the problem of impact by rigid or deformable indenter against a halfspace that precludes the possibility of analyzing the waves reflected from the boundaries of the impacted solid. Studies of indenter interaction with solids of finite size are much less represented. Positing such a problem appears topical in the practical aspect as well – in particular, in view of the wide use of laminate materials in modern aircraft and shipbuilding. It is noteworthy that scale effect is among the determinant qualitative factors for problems of stresses and fracture in impact interaction (see e.g. [14, 15]): the structure element under impact loading is destroyed by stresses whose level is formed due to superposition of waves reflected from boundary surfaces. The classical Hertz theory of collision is known to be applicable in dynamics at large time values, i.e. after the wave processes have faded in the solid. The Saint − Venant wave theory of rod collision is well developed only for quasi-onedimensional problems and does not take into account energy transfer in directions different from the impact direction. It is therefore necessary to develop more adequate models and investigation methods for dynamic processes of indentation.

The present publication is devoted to the construction of such approaches. As the object under impact *an elastic layer* is considered (plane statement) as the simplest body enabling the study of the character of the effect of multiply reflected waves on the formation of the stress state. This paper consists of two parts. In the first part a precise analytical solution is obtained about non-stationary indentation of a parabolic cylinder (with axis perpendicular to the problem plane) into the surface of an elastic layer. The character is determined of the development of stresses resulting from the superposition of the reflected waves at different physical and mechanical characteristics of the layer material.

In the second part a numerical solution is obtained on the basis of the so-called theory of elasticity with a single displacement. This model was introduced in [16] and used in a set of dynamical problems [5, 18, 19, 21, 22], in which one displacement predominates. The explicit finite difference algorithms are used together with the mesh dispersion minimization (MDM) approach, resulting in precise calculations of discontinuities. The MDM, originally created in [20] for homogeneous hyperbolic problems, then has been upgraded in [8–11, 13, 17] for computation of more complicated processes of wave and fracture propagation. MDM is based on a generalized concept of the Courant condition that relates mesh parameters to wave velocity, which reflects properties of the material at hand. Difference presentation of original differential equations exhibits some typical domains of influence, and the idea behind MDM is to properly adjust these domains so as to improve convergence. To this end, phase velocities of high-frequency components of the continuous models have to be considered, and the mesh to be set so that the propagation velocities induced by them approximate the former as closely as possible. An important technical advantage of MDM is that it utilizes the same mesh for both high-gradient and smoothed solution components. A satisfactory correspondence of analytical and computer solutions opens the way for using the latter to solve contact-impact problems, in which the indenter has an irregular contour. Calculation results are presented for dynamic pressing in of an indenter having a contour with angle points (rectangle, wedge and their combination). The stress and drag are calculated in dependence on time and the indenter parameters.

2. Problem statement. A rigid indenter at time $t = 0$ reaches the surface of elastic layer $z = 0$ and begins to press into it. The pressing-in process is specified by the indenter's velocity $V_0(t)$ perpendicular to the layer's surface. The impact velocity is assumed to be much less than that of the elastic waves in the layer, while the penetration depths are insignificant. This enables the formulation of a linear problem of theory elasticity, with the boundary conditions remaining valid for the undisturbed layer surface. We refer the layer to Cartesian coordinates x, z $(0 \le z \le h, -\infty < x < \infty)$, so that axis x is directed along the free surface and axis y into the layer (Fig. 1). Introduce dimensionless notations

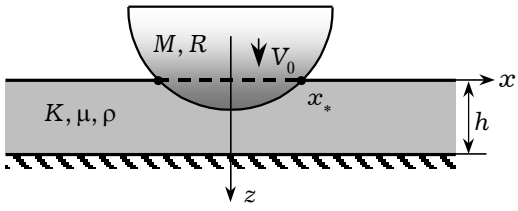

Fig. 1

$$\bar{x} = \frac{x}{R}, \quad \bar{z} = \frac{z}{R}, \quad \bar{t} = \frac{c_0 t}{R}, \quad \bar{w}_0 = \frac{w_0}{R}, \quad \bar{M} = \frac{M}{\gamma R^2}, \quad \bar{V}_0 = \frac{V_0}{c_0}, \quad c_0 = \sqrt{\frac{K}{\gamma}},$$

$$\bar{u}_j = \frac{u_j}{R}, \quad \alpha = \frac{c_p}{c_0}, \quad \beta = \frac{c_s}{c_0}, \quad b = \frac{\beta}{\alpha}, \quad \bar{\sigma}_{jk} = \frac{\sigma_{jk}}{K}, \quad j,k = x,z,$$

$$c_p = \sqrt{\frac{\lambda + 2\mu}{\gamma}}, \quad c_s = \sqrt{\frac{\mu}{\gamma}}, \quad K = \frac{3\lambda + 2\mu}{3} \qquad (1)$$

(the line above the notations will be omitted below). Here R is the characteristic linear dimension of the indenter, w_0 is its displacement counted from the undisturbed surface of the upper layer, V_0 and M are its movement velocity and mass respectively, c_p and c_s are respectively velocities of longitudinal and shear waves in the layer, γ is the density of the layer material, K is its uniform compression modulus, λ, μ are Lame's constants, u_j are components of the displacement vector, σ_{jk} are components of the stress tensor.

The behavior of the elastic medium is described by potentials Φ and Ψ, which in the case of a plane problem satisfy wave equations

$$\frac{\partial^2\Phi}{\partial x^2} + \frac{\partial^2\Phi}{\partial z^2} - \frac{1}{\alpha^2}\frac{\partial^2\Phi}{\partial t^2} = 0, \qquad \frac{\partial^2\Psi}{\partial x^2} + \frac{\partial^2\Psi}{\partial z^2} - \frac{1}{\beta^2}\frac{\partial^2\Psi}{\partial t^2} = 0 \tag{2}$$

and are connected with displacements and stresses by relationships

$$u_x = \frac{\partial\Phi}{\partial x} + \frac{\partial\Psi}{\partial z}, \qquad u_z = \frac{\partial\Phi}{\partial z} - \frac{\partial\Psi}{\partial x},$$

$$\sigma_{xx} = (1 - 2b^2)\frac{\partial^2\Phi}{\partial t^2} + 2\beta^2\left(\frac{\partial^2\Phi}{\partial x^2} - \frac{\partial^2\Psi}{\partial x\partial z}\right),$$

$$\sigma_{zz} = (1 - 2b^2)\frac{\partial^2\Phi}{\partial t^2} + 2\beta^2\left(\frac{\partial^2\Phi}{\partial z^2} - \frac{\partial^2\Psi}{\partial x\partial z}\right),$$

$$\sigma_{xz} = \beta^2\left(2\frac{\partial^2\Phi}{\partial x\partial z} + \frac{\partial^2\Psi}{\partial z^2} - \frac{\partial^2\Psi}{\partial x^2}\right). \tag{3}$$

The initial conditions for wave potentials are zero.

The boundary conditions of the problem are set on the front and back surfaces $z = 0$ and $z = h$. The boundary conditions at the layer front surface $z = 0$ are: equality of layer and indenter displacements normal to the surface in the contact zone, absence of normal stress σ_{zz} outside the contact zone and of tangential stress σ_{xz} (i.e. friction between layer and indenter)

$$u_z\big|_{z=0} = w_0(t), \qquad z = 0, \qquad |x| < |x^*|,$$

$$\sigma_{zz}\big|_{z=0} = 0, \qquad z = 0, \qquad |x| > |x^*|,$$

$$\sigma_{xz}\big|_{z=0} = 0, \qquad z = 0, \qquad |x| \geq 0. \tag{4}$$

Besides, it is necessary to see that stress σ_{zz} in the contact zone should remain compressing in the obtained solution:

$$\sigma_{zz}\big|_{z=0} > 0, \qquad |x| < |x^*|. \tag{5}$$

Normal displacements and shear stresses are zero at the layer back surface

$$u_z = 0, \qquad \sigma_{xz} = 0, \qquad z = h. \tag{6}$$

The boundaries of the contact zone will be the intersection points of the indenting body contour $x^*(t)$ and plane $z = 0$; if the surface of the moving body is set in the space of variables z, x, t by equation $z = F(t, x)$, the indicated points $x^*(t)$ will be the roots of equation

$$F(t, x) = 0. \tag{7}$$

System (1)–(7) formulates the problem of indenter and layer interaction at the given impact velocity.

3. Analytical solution. The formulated problem admits an analytical solution on the condition that the indenter contour is a sufficiently smooth, gently changing curve. Let the flatness of the indenter be such that at small times of interaction boundary point $x^*(t)$ under conditions (4) moves with velocity ex-

ceeding that of the elastic waves. As a result the latter do not emerge on the free layer surface, and conditions on boundary $z = 0$ are

$$\left.\frac{\partial u_z}{\partial t}\right|_{z=0} = H(x^* - x)V_0(t) = V_0(t,x), \quad \sigma_{xz}\big|_{z=0} = 0, \qquad x \geq 0. \tag{8}$$

Here $H(\cdot)$ is the Heaviside unit function. The condition on the back side remains unchanged

$$u_z\big|_{z=h} = 0, \qquad \sigma_{xz}\big|_{z=h} = 0. \tag{9}$$

The solution to be obtained here, apart from its independent significance, also serves below to test the numerical algorithm.

To solve problem (2), (8), (9) the Laplace integral transform in time with parameter s (upper index L) and the Fourier integral transformation with parameter ξ (upper index F) are used. In the image space the wave equations (with account taken of initial conditions) will take the form

$$\frac{\partial^2 \Phi^{LF}}{\partial z^2} - \left(\frac{s^2}{\alpha^2} + \xi^2\right)\Phi^{LF} = 0, \qquad \frac{\partial^2 \Psi^{LF}}{\partial z^2} - \left(\frac{s^2}{\beta^2} + \xi^2\right)\Psi^{LF} = 0, \tag{10}$$

while the boundary conditions will be as

$$su_z^{LF}\big|_{z=0} = \frac{1}{s}V_0^{LF}(s,\xi), \quad \sigma_{xz}^{LF}\big|_{z=0} = 0, \quad u_z^{LF}\big|_{z=h} = 0, \quad \sigma_{xz}^{LF}\big|_{z=h} = 0. \tag{11}$$

The general solution of equations (10) takes the following form:

$$\Phi^L = A(s,\xi)e^{-\frac{z}{\alpha}P} + \tilde{A}(s,\xi)e^{\frac{z}{\alpha}P}, \qquad \Psi^L = B(s,\xi)e^{-\frac{z}{\beta}S} + \tilde{B}(s,\xi)e^{\frac{z}{\beta}S},$$

$$P = \frac{\sqrt{s^2 + \alpha^2\xi^2}}{\alpha}, \qquad S = \frac{\sqrt{s^2 + \beta^2\xi^2}}{\beta}. \tag{12}$$

Here $A(s,\xi)$, $\tilde{A}(s,\xi)$, $B(s,\xi)$, $\tilde{B}(s,\xi)$ are the functions to be determined. By satisfying boundary conditions (11), the following expression is obtained for the image of normal stress σ_{zz}^{LF}:

$$\sigma_{zz}^{LF} = -\alpha V_0^{LF}(s,\xi)\cdot T(s,\xi), \tag{13}$$

where

$$T(s,\xi) = \frac{(s^2 + 2\beta^2\xi^2)^2}{s^3\sqrt{s^2 + \alpha^2\xi^2}}\left(\sum_{m=0}^{\infty} e^{-\frac{2mh+z}{\alpha}\sqrt{s^2+\alpha^2\xi^2}} + \sum_{m=0}^{\infty} e^{-\frac{2(m+1)h-z}{\alpha}\sqrt{s^2+\alpha^2\xi^2}}\right) -$$

$$- \frac{4\beta^3\xi^2\sqrt{s^2 + \beta^2\xi^2}}{\alpha s^3}\left(\sum_{m=0}^{\infty} e^{-\frac{2mh+z}{\beta}\sqrt{s^2+\beta^2\xi^2}} + \sum_{m=0}^{\infty} e^{-\frac{(2m+1)h-z}{\beta}\sqrt{s^2+\beta^2\xi^2}}\right). \tag{14}$$

Now function $V_0(t,x)$ is to be concretized. Assume that the front surface of the indenter in plane Ozx is parabolic, while the velocity of its pressing in is constant and equals some value V_0. Then it is easy to see that function $V_0(t,x)$ is the following:

$$V_0(t,x) = V_0 H(kt - x^2), \quad k = 2V_0, \quad V_0^{LF}(s,\xi) = V_0\sqrt{\frac{k}{2}}\frac{1}{s^{3/2}}e^{-\frac{\xi^2 k}{4s}}. \tag{15}$$

The problem thus consists in the conversion of expression (13), with functions T and V getting the forms of (14) and (15).

For stresses σ_{zz} on axis z (i.e. we set $x = 0$ in the Fourier image) we obtain

$$\sigma_{zz}^{L}(s,z,x=0) = -\alpha V_0 \sqrt{\frac{k}{\pi}} \frac{1}{s^{3/2}} \int_0^\infty e^{-\frac{\xi^2 k}{4s}} T(s,\xi)\, d\xi . \qquad (16)$$

Then we introduce substitution $s\eta = \xi$ and denote

$$Z_{mm\alpha} = \frac{2mh+z}{\alpha}, \qquad Z_{mp\alpha} = \frac{(2m+1)h-z}{\alpha},$$

$$Z_{mm\beta} = \frac{2mh+z}{\beta}, \qquad Z_{mp\beta} = \frac{(2m+1)h-z}{\beta}, \quad m = 0,1,\ldots,\infty,$$

$$R_{mm\alpha}(t,z) = \sqrt{4\alpha^2 kt + 4Z_{mm\alpha}^2\alpha^4 + k^2}\,,$$

$$T_{mm\alpha}(t,z) = kt + 2Z_{mm\alpha}^2\alpha^2 - Z_{mm\alpha}\sqrt{4\alpha^2 kt + 4Z_{mm\alpha}^2\alpha^4 + k^2}\,,$$

$$R_{mp\alpha}(t,z) = \sqrt{4\alpha^2 kt + 4Z_{mp\alpha}^2\alpha^4 + k^2}\,,$$

$$T_{mp\alpha}(t,z) = kt + 2Z_{mp\alpha}^2\alpha^2 - Z_{mp\alpha}\sqrt{4\alpha^2 kt + 4Z_{mp\alpha}^2\alpha^4 + k^2}\,,$$

$$R_{mm\beta}(t,z) = \sqrt{4\beta^2 kt + 4Z_{mm\beta}^2\beta^4 + k^2}\,,$$

$$T_{mm\beta}(t,z) = kt + 2Z_{mm\beta}^2\beta^2 - Z_{mm\beta}\sqrt{4\beta^2 kt + 4Z_{mm\beta}^2\beta^4 + k^2}\,,$$

$$R_{mp\beta}(t,z) = \sqrt{4\beta^2 kt + 4Z_{mp\beta}^2\beta^4 + k^2}\,,$$

$$T_{mp\beta}(t,z) = kt + 2Z_{mp\beta}^2\beta^2 - Z_{mp\beta}\sqrt{4\beta^2 kt + 4Z_{mp\beta}^2\beta^4 + k^2}\,.$$

Finally, after a series of transformations (omitted here), with the use of the convolution theorem in particular, we obtain

$$\sigma_{zz}(t,z) = -V_0 \frac{\alpha}{\pi k^2\sqrt{k}} \times$$

$$\times \left\{ \sum_{m=0}^{\infty} H(t - Z_{mm\alpha}) \int_{Z_{mm\alpha}}^{t} \frac{1}{\sqrt{t-\tau}} \frac{\left(k^2 + 8\beta^2 T_{mm\alpha}(\tau,z)\right)^2}{\sqrt{k^2 + 4\alpha^2 T_{mm\alpha}(\tau,z)}} \cdot \frac{1 - \dfrac{2\alpha^2 Z_{mm\alpha}}{R_{mm\alpha}(\tau,z)}}{\sqrt{T_{mm\alpha}(\tau,z)}}\, d\tau + \right.$$

$$+ \sum_{m=0}^{\infty} H(t - Z_{mp\alpha}) \int_{Z_{mp\alpha}}^{t} \frac{1}{\sqrt{t-\tau}} \frac{\left(k^2 + 8\beta^2 T_{mp\alpha}(\tau,z)\right)^2}{\sqrt{k^2 + 4\alpha^2 T_{mp\alpha}(\tau,z)}} \cdot \frac{1 - \dfrac{2\alpha^2 Z_{mp\alpha}}{R_{mp\alpha}(\tau,z)}}{\sqrt{T_{mp\alpha}(\tau,z)}}\, d\tau -$$

$$- \frac{16\beta^3}{\alpha} \sum_{m=0}^{\infty} H(t - Z_{mm\beta}) \int_{Z_{mm\beta}}^{t} \frac{\sqrt{T_{mm\beta}(\tau,z)}}{\sqrt{t-\tau}} \sqrt{k^2 + 4\beta^2 T_{mm\beta}(\tau,z)} \times$$

$$\times \left(1 - \frac{2\beta^2 Z_{mm\beta}}{R_{mm\beta}(\tau,z)} \right) d\tau - \frac{16\beta^3}{\alpha} \sum_{m=0}^{\infty} H(t - Z_{mp\beta}) \times$$

$$\left. \times \int_{Z_{mp\beta}}^{t} \frac{\sqrt{T_{mp\beta}(\tau,z)}}{\sqrt{t-\tau}} \sqrt{k^2 + 4\beta^2 T_{mp\beta}(\tau,z)} \left(1 - \frac{2\beta^2 Z_{mp\beta}}{R_{mp\beta}(\tau,z)} \right) d\tau \right\}. \qquad (17)$$

Formula (17) is obtained, which is a precise analytical expression for normal stress $\sigma_{zz}(t,z)$ at arbitrary point of the layer on axis z. It consists of four infinite sums: each m-th item of the first (second) sum represents the

m-th expansion wave reflected from the front (back) surface of the layer; each m-th item of the third (fourth) sum represents the m-th shear wave reflected from the front (back) surface of the layer. Keeping a finite number of items N in these sums, we obtain the value of stress with account taken of N reflections, which is the exact solution of the considered problem on the time interval $\frac{z}{\alpha} < t < \frac{2Nh + z}{\alpha}$.

Some results obtained with formula (17) are shown in Fig. 2–4. The indenter shape is given by expression (15), $V_0 = 0.01$, $a = 1$. To estimate the influence of shear rigidity on normal stresses in the layer, parameter β is varied. Here and below compression stresses are taken positive.

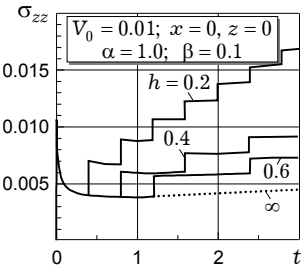

Fig. 2

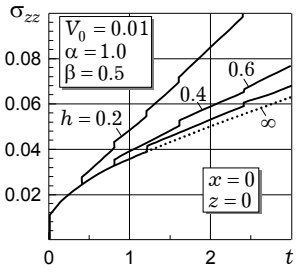

Fig. 3

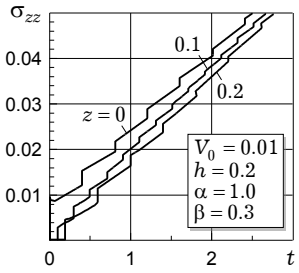

Fig. 4

Fig. 2 (relatively low shear rigidity $\beta = 0.1$) shows how the normal stress σ_{zz} at point $z = x = 0$ changes with time. Dimensionless thicknesses of the layer are $h = 0.2, 0.4$ and 0.6 (the dashed curve corresponds to an infinite layer). Stress $\sigma_{zz}(0,0) = V_0$ at the initial moment of interaction, once after that $\sigma_{zz}(0,0)$ decreases with time up to the moment of the first reflected wave incoming. Then a step-wise shape of σ_{zz} is realized due to following multiple reflections. The amplitudes of discontinuities (caused by fronts of reflected waves) are decreased after each reflection, and average values of $\sigma_{zz}(0,0)$ increase linearly with the course of time and inversely proportional to the normal rigidity of the layer or, which is the same, proportional to its thickness for the same Lame parameters.

The same process can be seen in Fig. 3, where stresses are depicted in the case of relatively high shear rigidity $\beta = 0.5$. A similar step-wise shape of $\sigma_{zz}(0,0)$ is observed in the comparison with the previous case, while the difference is that significant growth of $\sigma_{zz}(0,0)$ is realized once after the collision and preserved at the entire time interval. The above-mentioned linear dependence on time is realized, as well as the dependence of its slope on the layer thickness.

Normal stresses at three axial points: $z = 0$ (the front surface), $z = h/2$ (the layer middle) and $z = h$ (the back surface) are depicted in Fig. 4 corresponding to the layer of relatively median shear rigidity $\beta = 0.3$. The stress gaps are distinctly visible at moments of incoming wave fronts. The integral qualitative effects remain the same as in the previous cases.

4. Numerical solution. In this section, results of computer simulations are presented of the problem under consideration for some non-blunted shapes of the indenter with angle points. Such points are sources of singularity in stresses arising in the indentation process. To the best of the present authors' knowledge, closed analytical solutions are absent for the considered impact-

contact problems, while some asymptotic estimations exist and in the case of a halfspace can be found, for example, in [3, 6, 7]. As was shown in [7], normal stresses in the vicinity of the singular point (the punch edge) rise as

$$\sigma_{zz}(X,t)\big|_{z=0} \sim \frac{\ln(t)}{\sqrt{1-X^2}}, \qquad t \to \infty, \tag{18}$$

where X is the distance from the punch edge. Note that this square dependence is the same as in the static problem.

As was said above, in numerical formulation of the plane contact-impact problem we will use a simplified equation obtained from the plane problem of theory of elasticity by elimination of one of two displacements [16] (due to corresponding physical-geometrical assumptions). The more accurate formulation is that the following inequalities between stress components are fulfilled:

$$\frac{\partial u_z}{\partial z} \gg \frac{\partial u_x}{\partial x} \quad \Rightarrow \quad \sigma_{zz} \sim c_p^2 \gamma \frac{\partial u_z}{\partial z},$$

$$\frac{\partial u_z}{\partial x} \gg \frac{\partial u_x}{\partial z} \quad \Rightarrow \quad \sigma_{xz} \sim c_p^2 \gamma \frac{\partial u_z}{\partial x}. \tag{19}$$

As a result, displacement u_x is eliminated in the considered process of normal indentation, and the governing equation with respect to the normal displacement $u(x,z,t) \equiv u_z(x,z,t)$ (similar to the anti-plane one)

$$\ddot{u} = u''_{zz} + c_s^2 u''_{xx} \tag{20}$$

is obtained in the case of the modified plane problem.

Boundary conditions are modified now as

$$z = 0: \quad \dot{u} = V_0(x,t), \quad |x| \le x_*; \qquad \frac{\partial u}{\partial z} = 0, \quad |x| > x_*;$$

$$z = h: \quad u = 0.$$

Because we have a single displacement, shear boundary conditions at $z = 0$ and $z = h$ are not required now. In this simplified formulation neither longitudinal displacement u_x nor stress σ_{xx} are determined, while in the shear stress one of the components is absent. Under some systems of loading the considered model is in good correspondence with the original theory of elasticity. Below we compare the results obtained by this model with the analytical solution presented in Section 3. We note in advance that model (20) possesses higher rigidity in comparison with theory of elasticity; it can play the role of the upper estimate for the former. Note also that partial justification for this model can be found in the fact that it correctly described the qualitative relation (18) and its results obtained for a parabolic indenter have a good correspondence to the analytical solution. However, the main reason for its use is methodological: the explicit algorithm designed below and applied to the model allows front discontinuities and singular components of the solution to be calculated without parasite effects of mesh discretization. This point requires additional explanations.

A lot of computer algorithms are designed to solve similar contact-impact problems, while the question how to accurate describe wave fronts and high gradients still remains open. In diverse numerical tools including those used in so-called commercial hydrocodes (see, for example [12, 23, 24]), artificial viscosity is introduced to eliminate parasite oscillations arising in front vicinities (and fronts are spread together with them). Note that implicit schemes possessing an infinite influence domain (or dependence domain) are not intended for description of wave fronts at all. Thus, mesh dispersion, rather than the approximation problem, is the main obstacle for accurate calculations of contact-impact problems by explicit algorithms. Beginning from [18], the Mesh

Dispersion Minimization (MDM) algorithms are designed allowing the above-mentioned mesh effect to be significantly decreased or eliminated altogether. The latter was successfully realized in diverse 1D theoretical and practical problems [8–11, 13, 17, 19, 20], while 2D problems, to the best of the present authors' knowledge, were calculated without mesh dispersion only using a mixed numerical-analytical approach, in which one spatial coordinate was separated to a set of Fourier harmonics [9].

The MDM relates parameters of discrete mesh to wave velocities: the spatial step divided by the corresponding velocity is equal to the time step. To elucidate the main concept of the MDM, we present below an example of the simplest 1D wave equation, where such a procedure is completely realized. Let a semi-infinite straight elastic rod be subjected to a step stress on its end. Formulation of the problem is the following:

$$\ddot{u} = c_0^2 u'' \quad (c_0^2 = E/\rho); \qquad ESu'(0,t) = H(t); \quad u(x,0) = \dot{u}(x,0) = 0\,, \tag{21}$$

where E is Young's modulus, ρ is the density, S is the cross-section, c_0 (below $c_0 = 1$) is the sound velocity in the rod, u' and $\dot{u}$ are spatial and time derivatives. Dispersion relation obtained from (21) by Fourier analysis is

$$c = 1\,, \tag{22}$$

where c is the phase speed. The solution of (21) is of course dispersionless. Stresses, for example, are the following:

$$\sigma(x,t) \equiv Eu'(x,t) = \sigma_0 H(t-x)\,. \tag{23}$$

Problem (21) discretized by the explicit scheme is

$$\ddot{u} = u'' \;\Rightarrow\; u_i^{k+1} - 2u_i^k + u_i^{k-1} = \delta^2\left(u_{i+1}^k - 2u_i^k + u_{i-1}^k\right), \quad \delta = \Delta t/\Delta x\,,$$

$$Eu'(0,t) = \sigma_0 H(t) \;\Rightarrow\; u_{-1}^0 = u_0^0 + \Delta x\,\sigma_0\,,$$

$$u(x,0) = \dot{u}(x,0) \;\Rightarrow\; u_i^{-1} = u_i^0 = 0\,. \tag{24}$$

There $x = i\Delta x$, $t = k\Delta t$; Δx and Δt are spatial and temporal steps of the difference mesh, i and k are the coordinates of the current mesh node. The dispersion relation corresponding to the discrete case is

$$c = 1 \;\Rightarrow\; c = \pm\frac{2}{q\Delta t}\arcsin\left(\delta\cdot\sin\frac{q\Delta x}{2}\right), \tag{25}$$

where q is the wavelength. It can be seen that phase speed c depends on the wavelength here: waves do propagate dispersionally.

The dispersion equation (25) has an infinity of modes that relate to *arcsin* periodicity. However, if $\Delta x = \Delta t$ ($\delta = 1$), dispersion relation (22) and its discrete analog (25) coincide. Thus in this case the discrete solution turned out to be also dispersionless. Remind that equality $\delta = 1$ is the limiting value of the Currant stability criterion: $\delta \le 1$. Discrete equation (24) in case $\delta = 1$ is rewritten as

$$u_i^{k+1} = u_{i+1}^k + u_{i-1}^k - u_i^{k-1}, \quad u_{-1}^0 = u_0^0 + \Delta x\sigma_0, \quad u_i^{-1} = u_i^0 = 0\,. \tag{26}$$

Its solution

$$\sigma_i^k = \begin{cases} \sigma_0, & i \le k, \\ 0, & i > k, \end{cases} \tag{27}$$

which is analytically obtained by induction, coincides with the D'Alambert analytical solution (22) in the mesh nodes. So, mesh dispersion is eliminated in scheme (26). This simple example is at the basis for the MDM technique. The MDM principle rule – influence domains of continual and discrete equations

must be as close as possible – preserves in more complicated problems. As to model (20) possessing two influence domains, $r \equiv \sqrt{x^2 + y^2} = c_p t$ and $r = c_s t$, it is impossible to obtain the same domains in its discrete analog built by conventional homogeneous algorithms. However, a special presentation of discrete derivatives results in an MDM algorithm allowing domain $z = c_p t$ to be superposed in continual and discrete models. This way is presented below.

First, due to the problem symmetry we consider a quarter of the plane. Similar to the simplest example (24) we denote Δt, Δz and Δx as 3D mesh steps, $t = k\Delta t$, $z = j\Delta z$ and $x = i\Delta x$, where $k = 0,\dots,K$, $i = 0,\dots,I$ and $j = 0,\dots,J$, $J = h/\Delta z$. Integer K and I will be chosen from a condition of absence of influence of artificial boundary $x = I\Delta x$ on the xzt-domain of interest. For second derivations from (20) we use following discretizations:

$$\ddot{u} \sim (u_{j,i}^{k+1} - 2u_{j,i}^{k} + u_{j,i}^{k-1})\frac{1}{(\Delta t)^2},$$

$$u''_{zz} \sim (u_{j+1,i}^{k} - 2u_{j,i}^{k} + u_{j-1,i}^{k})\frac{1}{(\Delta z)^2},$$

$$u''_{xx} \sim (U_{j,i+1}^{k} - 2U_{j,i}^{k} + U_{j,i-1}^{k})\frac{1}{(\Delta x)^2},$$

$$U_{j,i}^{k} = \frac{1}{4}(u_{j+1,i}^{k} + 2u_{j,i}^{k} + u_{j-1,i}^{k}), \qquad (28)$$

in which the first two are conventional explicit, while the third is written relatively a median value $U_{j,i}^{k}$ for the three nearest points on the z-axis. As can be seen, the accuracy level of calculations ($\sim((\Delta t)^2 + (\Delta z)^2 + (\Delta x)^2)$) in the discrete analog of (20) built with (28) remains the same as in a conventional case (i.e. in the case $U_{j,i}^{k} \equiv u_{j,i}^{k}$). For a system of closed 1D equations the approximation similar to (28) was originally introduced in [5]. As far as the present authors know, such algorithms for 2D spatial problems have not yet been designed.

The dispersion equation for continual model (19) is

$$\omega = \sqrt{c_p^2 q_z^2 + c_s^2 q_x^2} \qquad (29)$$

(ω is the frequency, q_x and q_z are components of the wave vector), while for its discrete analog with (28) taken into account we have

$$\sin\frac{\omega\Delta t}{2} = \Delta t\sqrt{\frac{c_p^2}{(\Delta z)^2}\sin^2\frac{q_z\Delta z}{2} + \frac{c_s^2}{(\Delta x)^2}\sin^2\frac{q_x\Delta x}{2}\cdot\cos^2\frac{q_z\Delta z}{2}}. \qquad (30)$$

If $\delta_z \equiv \Delta t/\Delta z = 1$ is taken, waves of the minimal short length in z-direction propagate with the maximal speed $c = c_p$. The minimal length including three mesh nodes is $\lambda_z = 2\Delta z$, while the minimal wave number is $q_z \equiv 2\pi\frac{1}{\lambda_z} =$ $= \pi\frac{1}{\Delta z}$. Notably short waves form front discontinuities. In a case similar to the one considered, when front discontinuities propagate along a single direction, such fronts are to be precisely calculated. The designed scheme is stable at $\Delta z = c_p\Delta t$ independently from Δx.

Below we present a set of results calculated by discrete model (20) with approximation (28) for indentation of a layer by punches of finite width 2ℓ

and various contours of the indenter head. First, an indenter with parabolic contour is considered to compare analytical and numerical solutions. In Fig. 5*a* the problem geometry is shown, while in Fig. 5*b* dependences $\sigma_{zz}(x,0)$ vs. time are depicted at the layer surface $z = 0$ in points $x = 0$, 0.04 and 0.1. The layer thickness is taken $h = 0.2$, the punch width is infinite ($\ell \sim \infty$), $\alpha = 1$ and $\beta = 0.5$ – all the parameters are the same as were chosen in the analytical solution shown in Fig. 3. Steps of the difference mesh are $\Delta x = \Delta z = \Delta t = 0.002$ (recall that the numerical approach determines the average stress acting on an area with length equal to the spatial step).

The comparison shows a good correspondence of two approaches. The computer solution (curve for $x = 0$, Fig 5*b*) turns out higher by ~2% than that in the analytical one (curve for $h = 0.2$, Fig 3) at the common time interval. However, as comparisons show, in cases of low β this convergence is more significant and increases if β decreases. This fact can be explained by too high common rigidity of the simplified model.

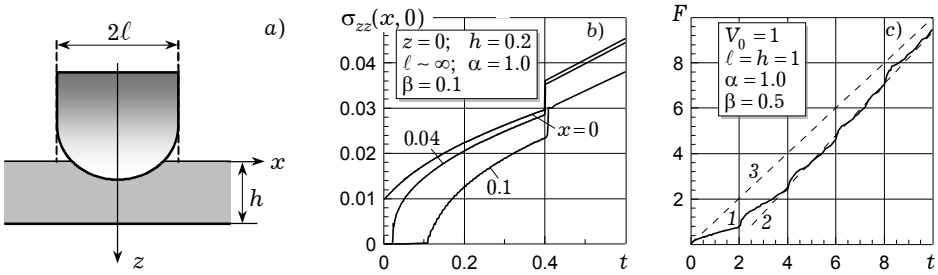

Fig. 5

Note that in practice, not stresses but the drag is the more required parameter. The drag shown in Fig 5*c* – solid line *1* – is normalized by the punch length: $F(k\Delta t) = \frac{1}{\ell} \sum_{i=0}^{i=\ell/\Delta x} \frac{\sigma_{0,i}(k\Delta t)}{V_0}$. As can be seen, the average value of F is approached by a straight line *2* once after one-two reflections. Comparison with the drag obtained in the case of the simplest 1D spring model of the effective rigidity equal to $\gamma c_p^2 \ell / h$ (straight line *3*) shows that an insignificant divergence is observed in the considered cases. So, in practice the latter very rough estimate can be used for the drag formed after multiple reflections. In results presented in Fig 5*c* and all the figures below we use punch width ℓ as the length measurement unit, while stresses are normalized by punch velocity V_0. Besides, layer parameters $\alpha = 1$ and $\beta = 0.5$ are taken. We also show results related to the positive part of the plane, only implying that the same dependencies relate to the negative part due to the symmetry.

The calculation results shown in Fig. 6 are related to indentation of the plane punch into the semi-infinite layer. The problem geometry is depicted in the inset. In Fig. 6*a* dependences of normal stresses $\sigma_{zz}(0,0)$, $\sigma_{zz}(0.5\ell,0)$ and drag F vs. time are depicted, while in Fig. 6*b* dependences $\sigma_{zz}(x,0)$ vs. time are depicted in the contact surfaces $z = 0$ in the vicinity of singular point $x = 0.9, 0.95, 0.98, 0.99, 1.0$. As calculations show, the distribution of stresses in the edge vicinity approaches (with time) asymptotic dependence (18). Thus, we can suppose that the simplified model used here is justified within the field of the taken parameters of the problem.

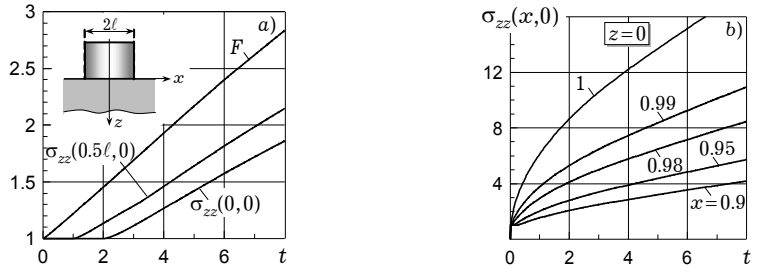

Fig. 6

Normal stresses in the contact surface $z = 0$ and drag $F(t)$ are depicted in Fig. 6 (a semi-infinite layer) and Fig. 7 (a finite thickness $h = 1$). Stresses σ_{zz} vs. time at several points in the contact surface $z = 0$, $x = 0, 0.5, 0.9$ and drag F are shown in Fig. 7*a*, and stresses in the vicinity of singular point $z = 0$, $x = 0.95, 0.99, 1.0$ – in Fig. 7*b*. Influence of the singularity at punch edge $x = \ell$ results in a significant growth of altitudes with time, while reflections intensify this process. A rapid rise of stresses at singular points and discontinuities at moments of incoming of reflected waves can be seen.

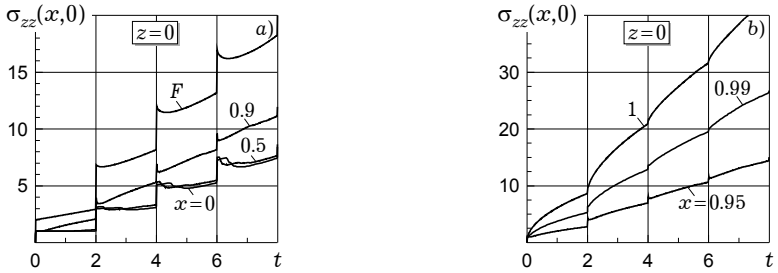

Fig. 7

For plane punch acted onto a semi-infinite layer ($h \sim \infty$) in Fig. 8 and 9 distributions of σ_{zz} are shown in the layer along axes x (in several z-cross-sections: $z = 0, 0.05, 0.1, 0.25, 0.5, 1, 2, 3, 5, 6$) and along axes z (in three vertical cross-sections $x = 0, 0.5, 1$) for some moments of time ($t = 1, 3, 6$). Maximal amplitudes of stresses reaching in the singular point are shown in upper left corners.

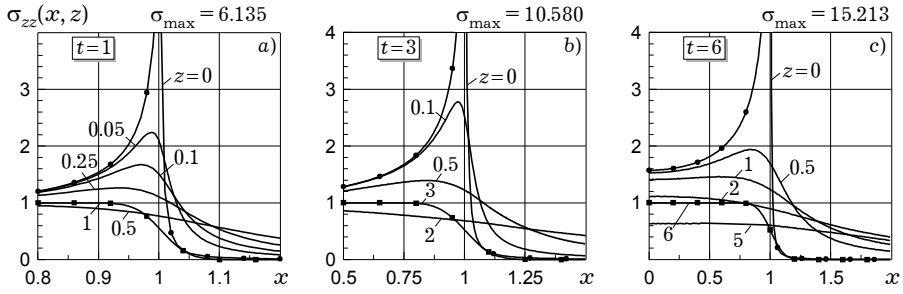

Fig. 8

Stresses σ_{zz} decrease with their propagation from the source (due to the wave divergence). In addition, a set of qualitative effects is observed caused by a complexity of the acting source – the continuous interaction of a constant initial force at the punch base and increasing forces at the vicinity of punch edges. Stress distribution $\sigma_{zz}(x, z_i)$ along the x-direction in various z-cross-sections of the layer relatively close to the face surface $z = 0$ is qualita-

tively similar to that observed in $z = 0$, the difference is that in $z = 0$ the vicinity of the projection of the singular point $x = 1$ the stress altitude rapidly decreases (Fig. 8), while its maximum moves from the edge to the punch median. Along with wave propagation deep into the layer, x-distribution of σ_{zz} is continuously spread, the altitude of σ_{zz} decreases in the vicinity of cross-section $x = 1$ and increases with approaching the axis of symmetry $x = 0$. This process is arrested in a small (decreasing with time) domain behind the front $z = c_p t$. At the front itself $\sigma_{zz} = 1$, and the influence of punch edges is absent, except for a small vicinity of the projection of singular point $x = 1$, where stresses rapidly decrease up to zero. It can been seen, with distributions in Fig. 9 in mind, that σ_{zz} propagation across the layer is similar to a quasi-stationary process.

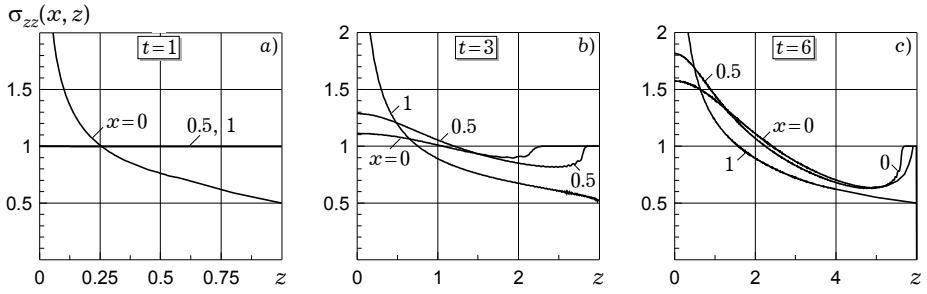

Fig. 9

Calculation results related to wedge indentation into a semi-infinite layer are presented in Fig. 10, $\ell = 1$ (the problem geometry is shown in the inset in Fig. 10*b*). The problem formulation corresponds to the case when the external loading (normal velocity) appears at the moment $t = 0$ at point $(0, 0)$ and then moves along the surface $z = 0$ with constant speed. The latter is determined by the value of the wedge shape. Let $æ = \mathrm{tg}\,\varphi$, where φ is half of the angle at the wedge apex, then the speed of the moving loading is $V_0 = æ$.

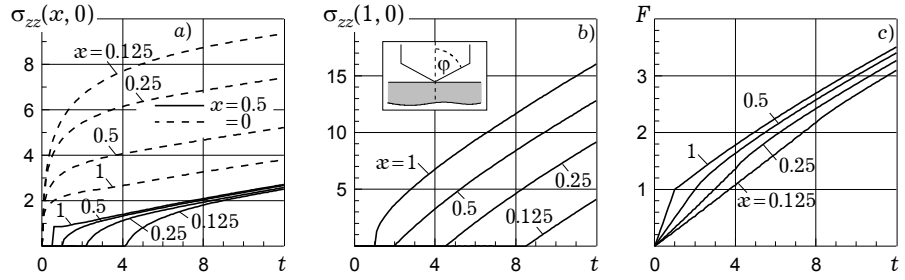

Fig. 10

Stresses $\sigma_{zz}(x, 0)$ and drag F vs. time are depicted for a set of wedge angles at some points of the contact surface. The problem has three singular points: $x = 0, 1$ and -1. Interaction of stresses radiating from these points determines the main peculiarities of the wave process. The smaller $æ$, the higher the contribution of singularity at $x = 0$ (the wedge apex) and the lesser at $x = 1$ (the wedge edge). A surprising result is a relatively weak dependence of the drag on $æ$. As was said above, the reason for it is the complicated character of interacting stresses at the contact surface.

In Fig. 11 and Fig. 12 analogous results are shown in the case of a partially truncated wedge of a finite width. The problem geometry can be seen in Fig. 11*a*. There are four singular points are: $x = \pm 0.2$ and $x = \pm 1$.

The stress pattern and drag vs. time are shown in Fig. 11*b* up to the time when reflections from the layer back appear. Note that a self-similar part of the wave process is clearly observed here: the same constant stress amplitude equal to 0.8667 is revealed in points at the contact surface up to the moment when the influence appears of waves radiating from singular points.

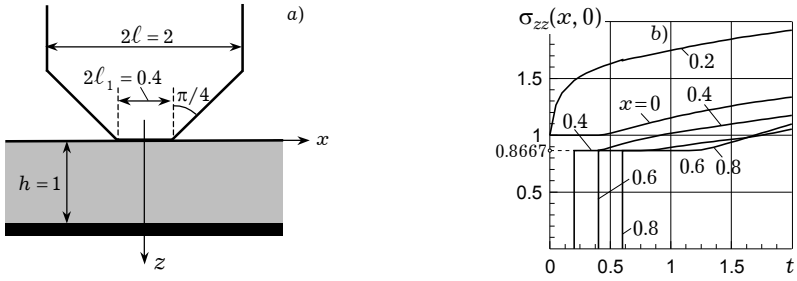

Fig. 11

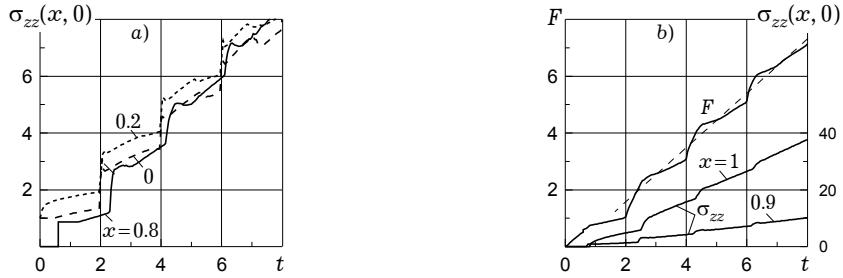

Fig. 12

In Fig. 12 stresses at some points of the contact surface and drag are depicted within the time interval including multiple reflections. Significant influence of wave fronts is preserved at internal points of the contact surface at the entire shown time interval, while at points close to the edge stress curves behave as gradually smoothed. The drag, as in the case of the spherical shape of the indenter head, is approached by the same straight line (compare dashed curves in this figure and in Fig. 5c).

1. *Горшков А. Г., Тарлаковский Д. В.* Динамические контактные задачи с подвижными границами. – Москва: Физматгиз, 1995. – 352 с.
2. *Кубенко В. Д.* Удар затупленных тел о поверхность жидкости или упругой среды // Прикл. механика. – 2004. – **40**, № 11. – С. 3–44.
3. *Лобысев В. Л., Яковлев Ю. С.* Поля напряжений при движении поршня с жестким фланцем на границе с идеально упругой средой // Механика твердого тела. – 1971. – № 4. – С. 65–69.
4. *Механика* контактных взаимодействий / Под ред. И. И. Воровича, В. М. Александрова. – Москва: Физматгиз, 2001. – 670 с.
5. *Ормонбеков Т.* Механика взаимодействия деформируемых тел. – Фрунзе: Илим, 1989. – 227 с.
6. *Поручиков В. Б.* Методы динамической теории упругости. – Москва: Наука, 1986. – 328 с.
7. *Слепян Л. И., Яковлев Ю. С.* Интегральные преобразования в нестационарных задачах маханики. – Ленинград: Судостроение, 1980. – 343 с.
8. *Abdukadyrov S. A., Pinchukova N. I., Stepanenko M. V.* A numerical approach to solving dynamic equations of elastic media and structures // Sov. Mining Sci. – 1984. – **21**, No. 6. – P. 34–41.
9. *Abdukadyrov S. A., Pinchukova N. I., Stepanenko M. V.* Nonstationary diffraction of plane longitudinal wave on an elastic cylindrical shell // Mechanics of Solids. – 1989. – **24**, 5. – P. 136–142.
10. *Ayzenberg-Stepanenko M. V.* Wave propagation and fracture in elastic lattices and composites // Personal Armour Systems. – London: British Crow Copyright, 1998. – P. 405–415.
11. *Ayzenberg-Stepanenko M. V., Sher E. N.* Modeling wave processes in periodic structures // J. Phys. Mesomech. – 2007. – **1**. – P. 34–43.

12. *Bajer A., Demkowicz L.* Dynamic contact/impact problems, energy conservation, and planetary gear trains // Comput. Meth. Appl. Mech. and Eng. – 2002. – **191**, No. 37-38. – P. 4159–4191.
13. *Gordienko V. I., Kubenko V. D., Stepanenko M. V.* Effect of a nonstationary internal wave on an elastic cylindrical shell // Sov. Appl. Mech. – 1981. – **17**, No. 3. – P. 245–249.
14. *Maekava I.* Size effect of impact strength and related applications // Size scale effects in the failure mechanisms of materials and structures / Ed. A. Carpenteri. – London: E&FN SPONS, 1996. – P. 567–573.
15. *Maekava I.* The influence of stress wave on the impact fracture strength of cracked member // Int. J. Impact Eng. – 2005. – **24**. – P. 1–4.
16. *Rakhamatullin H. A.* On propagation of elastic-plastic waves in a halfspace // Appl. Math. Mech. (ПММ). – 1959. – **23**. – P. 79–86.
17. *Slepyan L. I., Ayzenberg-Stepanenko M. V.* Localized transition waves in bistable-bond lattices // J. Mech. Phys. Solids. – 2004. – **52**. – P. 1447–1479.
18. *Smirnov A. L.* Impact penetration of piles into a soil // Sov. Mining Sci. – 1989. – **4**. – P. 47–59.
19. *Smirnov A. L., Yungerman L. N.* Elastic waves and oscillations in structures embedded in elastic halfspace // Theory of wave propagation in elastic and elastic-plastic solids / Ed. M. V. Stepanenko. – Novosibirsk, 1986. – Vol. 2. – P. 96–99.
20. *Stepanenko M. V.* Computing the pulsed strain processes in elastic structures. – 1976. – **12**, No. 2. – P. 53–57.
21. *Stepanenko M. V.* Dynamics of the fracture of unidirectional glass-plastic // J. Appl. Mech. Techn. Phys. – 1979. – **9**, No. 4. – P. 155–163.
22. *Stepanenko M. V.* Numerical experiment on the fracture dynamics of a composite material // Mech. Composite Materials. – 1981. – **1**. – P. 46–51.
23. *Wang F.-J., Wang L.-P., Cheng J.-G., Yao Z.-H.* Contact force algorithm in explicit transient analysis using finite-element method // Finite Elements in Analysis and Design. – 2007. – **43**, No. 6-7. – P. 580–587.
24. *Zhong Z.-H., Mackerie J.* Contact-impact problems: A review with bibliography // Appl. Mech. Rev. – 1994. – **47**, No. 2. – P. 55–76.

УДАРНЕ ВДАВЛЮВАННЯ ТВЕРДОГО ТІЛА В ПРУЖНИЙ ШАР. АНАЛІТИЧНИЙ І ЧИСЕЛЬНИЙ ПІДХОДИ

Розглядається плоска контактна задача для пружного шару, який піддається удару твердим індентором, що рухається із заданою швидкістю. У випадку затупленого індентора одержано точний аналітичний розв'язок задачі. Результати наведено для напруження як функції часу для шару скінченної товщини. Аналізується зміна напруження в результаті багатократних відбить хвиль. Чисельний розв'язок цієї задачі отримано на базі спрощеного варіанту теорії пружності з одним переміщенням. Розвинуто скінченнорізницевий алгоритм розрахунків на основі техніки мінімізації чисельної дисперсії, що підвищує точність обчислень в околі розривів функцій. Обчислені напруження і силу опору представлено для кількох нерегулярних форм індентора (прямокутник, клин і їх комбінації).

УДАРНОЕ ВДАВЛИВАНИЕ ТВЕРДОГО ТЕЛА В УПРУГИЙ СЛОЙ. АНАЛИТИЧЕСКИЙ И ЧИСЛЕННЫЙ ПОДХОДЫ

Рассматривается плоская контактная задача для упругого слоя, подверженного удару твердым, движущимся с заданной скоростью, индентором. В случае затупленного индентора получено точное аналитическое решение. Результаты представлены для напряжения как функции времени для слоя конечной толщины. Анализируется изменение напряжения в результате многократных отражений волн. Численное решение этой задачи получено на основе упрощенного варианта теории упругости с одним перемещением. Развит конечноразностный алгоритм расчетов, опирающийся на технику минимизации численной дисперсии, что повышает точность вычислений в окрестности разрывов функций. Вычисленные напряжения и сила сопротивления представлены для нескольких нерегулярных форм индентора (прямоугольник, клин и их комбинации).

[1] Timoshenko Inst. of Mechanics of NAS of Ukraine, Kiev,
[2] Ben-Gurion Univ. of the Negev, Be'er-Sheva, Israel

Received 11.01.08